ELSEVIER

International Journal of Mass Spectrometry 195/196 (2000) 271–284

International Journal of Mass Spectrometry

Microcanonical analysis of the kinetic method. The meaning of the "effective temperature"

Kent M. Ervin*

Department of Chemistry and Chemical Physics Program, University of Nevada, Reno, NV 89557, USA

Received 7 June 1999; accepted 17 August 1999

Abstract

An analytical expression for the "effective temperature" parameter in the Cooks kinetic method is derived using classical Rice–Ramsperger–Kassel (RRK) theory for the microcanonical unimolecular dissociation rate. The approximate expression is appropriate for metastable ion dissociation experiments and high ion source temperatures. The effective temperature is directly proportional to the well depth (complexation energy) of the dissociating cluster ion, is inversely proportional to the number of oscillators of the cluster (vibrational degrees of freedom), and also depends on the product of the reaction frequency (preexponential factor) and the instrumental time window of the experiment. Numerical simulations using classical RRK rates with a detailed kinetics treatment are compared with the analytical expression for the effective temperatures. For fast dissociations (shallow cluster well depth or small number of oscillators), threshold effects cause significant curvature in the kinetic method plots. The implications of these results on the accuracy of relative thermochemical measurements by the kinetic method are discussed. (Int J Mass Spectrom 195/196 (2000) 271–284) © 2000 Elsevier Science B.V.

Keywords: Kinetic method; Proton-bound dimers; Microcanonical kinetic rate theory

1. Introduction

The "kinetic method" originally developed by Cooks and co-workers is a widely used mass spectrometric technique for obtaining relative thermochemical information about ion–molecule systems [1–3]. In the kinetic method, the metastable or collision-induced decomposition of a mass-selected cluster ion that has two product channels is monitored in a tandem mass spectrometer, for example, the dissociation of a proton-bound anion $A_1HA_2^-$ as shown in Reactions (1) and (2).

$$A_1HA_2^- \rightarrow A_1^- + HA_2 \qquad (k_1) \tag{1}$$

$$\rightarrow HA_1 + A_2^- \qquad (k_2) \tag{2}$$

Fig. 1 shows an energy diagram for the dissociation. A correlation between the ratio of the intensities of the two product ions and the enthalpy or Gibbs free energy difference of the two product channels is made according to Eq. (3),

$$\ln \frac{I_2}{I_1} \approx -\frac{\Delta\Delta H}{RT_{\text{eff}}} \approx -\frac{\Delta\Delta G}{RT_{\text{eff}}} \tag{3}$$

* E-mail: ervin@chem.unr.edu

Dedicated to the memory of Professor Robert R. Squires.

PII S1387-3806(99)00176-1

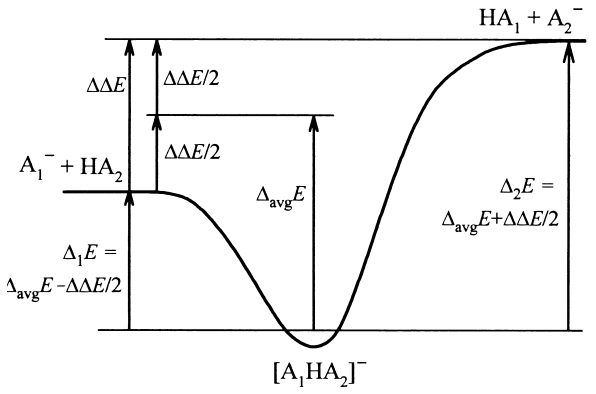

Fig. 1. Energy diagram of the dissociation of a proton-bound dimer anion.

where I_j is the measured intensity of ion A_j^-, $\Delta\Delta H = \Delta_2 H - \Delta_1 H$, $\Delta\Delta G = \Delta_2 G - \Delta_1 G$, and R is the gas constant. The "effective temperature," T_{eff}, is a correlation parameter determined from the slope of a plot of $\ln(I_2/I_1)$ versus $\Delta\Delta H$ or $\Delta\Delta G$. By measuring the product intensity ratios for proton-bound dimers composed of partners of known acidity, the slope of the correlation is found and then the acidity of an unknown can be measured versus one or more of the reference acids. In addition to proton-bound dimer ions, a variety of other types of clusters have been investigated by the kinetic method to determine other thermochemical quantities [2,3], including, for example, electron affinities from electron-bound dimers in experiments by the late Professor Robert R. Squires and his co-workers [4,5].

Various theoretical formulations have been presented to justify the correlation given by Eq. (3) [1,2,6–13], but its use and the meaning of the effective temperature parameter remain points of active discussion [13–18]. This work presents a microcanonical kinetics analysis of the kinetic method using the classical RRK (Rice–Ramsperger–Kassel) theory [19,20] of statistical unimolecular dissociation. I derive a simple analytical expression for the effective temperature for the case of metastable ion dissociation. The expression is compared with explicit calculations of the effective temperature using methods similar to those of Bojeson and Breindahl [8]. The implications for the accuracy of kinetic method measurements are discussed.

2. Canonical formulation

The correlation of Eq. (3) was originally and is most commonly justified using canonical transition state theory [1,2]. It is first assumed that the ratio of the ion intensities observed for the two channels is equal to the ratio of the macroscopic rate coefficients, as given by Eq. (4).

$$\frac{I_2}{I_1} \approx \frac{k_2(T)}{k_1(T)} \tag{4}$$

The rates for the competing decomposition channels, $j = 1$ and 2, are calculated by canonical transition state theory [19,20], Eq. (5),

$$k_j(T) = \frac{k_B T}{h} \frac{Q_j^{\ddagger}(T)}{Q_0(T)} e^{-\Delta_j E_{0K}^{\ddagger}/RT} \tag{5}$$

where T is temperature, h is Planck's constant, k_B is Boltzmann's constant, $Q_j^{\ddagger}(T)$ is the partition function for the transition state leading to channel j, $Q_0(T)$ is the partition function for the cluster ion, and $\Delta_j E_{0K}^{\ddagger}$ is the energy difference between the cluster and the transition state at zero temperature. The rate coefficient, $k(T)$, strictly applies to a canonical ensemble of reactant molecules, i.e. a system in thermal equilibrium at temperature T. Taking the logarithm of the ratio of the rate coefficients for the two channels, one obtains Eq. (6),

$$\ln \frac{k_2(T)}{k_1(T)} = -\frac{\Delta_2 E_{0K}^{\ddagger} - \Delta_1 E_{0K}^{\ddagger}}{RT} + \ln \frac{Q_2^{\ddagger}(T)}{Q_1^{\ddagger}(T)} \tag{6}$$

which contains no additional approximations beyond those of transition state theory [19,20]. One further assumes (1) there are no reverse activation energies [$\Delta_j E_{0K}^{\ddagger} = \Delta_j E_{0K}$], (2) the entropy differences between the two channels are zero [$\Delta\Delta S = R \ln(Q_2/Q_1) = 0$] or else $\Delta\Delta S$ is the same for all dimer pairs where $\Delta\Delta S = \Delta_2 S - \Delta_1 S$, and (3) the integrated heat capacity and entropy differences between internal energy, enthalpy, and Gibbs energy at various

temperatures are equal for the two channels and cancel [$\Delta\Delta E_{0K} = \Delta_2 E_{0K} - \Delta_1 E_{0K} \approx \Delta\Delta H_T \approx \Delta\Delta G_T$]. With these approximations, one obtains Eq. (7)

$$\ln \frac{k_2(T)}{k_1(T)} \propto -\frac{\Delta\Delta H}{RT} \approx -\frac{\Delta\Delta G}{RT} \tag{7}$$

Because the clusters in an ion beam are isolated species, not in thermodynamic equilibrium at any temperature, the temperature in Eq. (7) is replaced by the effective temperature T_{eff}. Finally, combining Eqs. (4) and (7) yields Eq. (3).

3. Approximate microcanonical derivation

Once an ion leaves the ion source of a mass spectrometer (or undergoes its last collision), it is isolated and its total internal energy, E, is conserved. Thus, the decomposition process is properly described by the microcanonical rate coefficient, $k(E)$, rather than by the canonical rate coefficient, $k(T)$. In a metastable ion dissociation experiment using a tandem mass spectrometer, the products are detected if the cluster ion lifetime falls within a narrow time window corresponding to the field-free region between the two mass-selection regions. For a sector instrument, a typical time window is defined by times of flight from the ion source of 20 μs to 40 μs. Ions with shorter lifetimes (higher internal energies) dissociate in the first mass-selection region and are ejected. Ions with longer lifetimes (lower internal energies) do not dissociate before the second mass-selection region. Assuming that the ions that dissociate within the time window of a tandem mass spectrometer have a single internal energy $E = E_d$, the measured ion intensity ratio is given by Eq. (8),

$$\frac{I_2}{I_1} \approx \frac{k_2(E_d)}{k_1(E_d)} \tag{8}$$

which is the microcanonical equivalent of Eq. (4).

Classical RRK theory, also known as classical quasiequilibrium theory (QET), provides a useful approximation for calculating the microcanonical unimolecular dissociation rate. Although the RRK model is inadequate for quantitative calculation of absolute rates, it is a simple analytical function that reproduces the essential behavior of the unimolecular dissociation rate as a function of internal energy. The RRK rate constant $k_j(E)$ for channel $j = 1$ or 2 is given by Eq. (9) [19,20],

$$k_j(E) = \nu\left(\frac{E - \Delta_j E^{\ddagger}_{0K}}{E}\right)^{s-1} \tag{9}$$

where s identical classical harmonic oscillators of frequency ν comprise the dissociating molecule. As with the canonical derivation, it is assumed that there are no reverse activation energies, $\Delta_j E^{\ddagger} = \Delta_j E$. The frequency factor and number of oscillators is the same for both channels, which is equivalent to assuming that $\Delta\Delta S = 0$. The classical RRK model tends to underestimate rates, so the number of oscillators s is often empirically reduced by a factor of 2–5 [8,19,20].

The next task is to derive the effective temperature parameter that would be *observed* in a metastable ion experiment. Evaluating the ratio of rates using the RRK model gives Eq. (10),

$$[k_2(E_d)/k_1(E_d)] = \left(\frac{E_d - \Delta_2 E}{E_d - \Delta_1 E}\right)^{s-1} = \left(\frac{E_d - \Delta_{avg} E - \Delta\Delta E/2}{E_d - \Delta_{avg} E + \Delta\Delta E/2}\right)^{s-1} \tag{10}$$

where the explicit $T = 0$ K subscripts have been dropped. Following Bojeson and Breindahl [8] and Brauman and co-workers [11], on the right-hand side of Eq. (10) the dissociation energies of the two channels are redefined in terms of the average dissociation energy $\Delta_{avg} E = (\Delta_1 E + \Delta_2 E)/2$ and the difference $\Delta\Delta E = \Delta_2 E - \Delta_1 E$ (see Fig. 1). The effective temperature can be found from the slope of the logarithm of the rate constant ratio versus $\Delta\Delta E$ ($\approx \Delta\Delta H$), as given in Eq. (11).

$$\frac{d \ln(k_2/k_1)}{d(\Delta\Delta E)} \equiv -\frac{1}{RT_{eff}} \tag{11}$$

Evaluating the derivative of $\ln(k_2/k_1)$ from Eq. (10) with respect to $\Delta\Delta E$ and solving for T_{eff} gives Eq. (12),

$$T_{\text{eff}} = \frac{(E_{\text{d}} - \Delta_{\text{avg}}E)^2 - (\Delta\Delta E/2)^2}{R(s-1)(E_{\text{d}} - \Delta_{\text{avg}}E)} \tag{12}$$

which indicates that the effective temperature and slope depends on $\Delta\Delta E$, i.e. the kinetic method plots are nonlinear in general. If $E_{\text{d}} - \Delta_{\text{avg}}E \gg \Delta\Delta E/2$, however, then the expression in Eq. (12) simplifies to Eq. (13).

$$T_{\text{eff}} \approx \frac{E_{\text{d}} - \Delta_{\text{avg}}E}{R(s-1)} \tag{13}$$

The simplifying assumption requires that the excess internal energy be much greater than the energy difference between the two channels, which is of doubtful generality. The range of its validity will be discussed below. An expression similar to Eq. (13) was derived by Beauchamp and co-workers [9], who stated that the effective temperature is proportional to the excess internal energy per degree of freedom. That definition of the effective temperature is valid, but it provides no guidance as to what the excess internal energy actually is for the observed dissociating ions.

The most probable value of the internal energy of the dissociating ions, E_{d}, in a metastable ion experiment can be found in the following manner. The observation of dissociation within the field-free region is most likely if the total dissociation rate matches the time window, Eq. (14),

$$\frac{1}{\tau} = k_1(E_{\text{d}}) + k_2(E_{\text{d}}) \tag{14}$$

where τ is the instrumental time for metastable ion dissociation and E_{d} is the ion internal energy required for the rate expression to satisfy Eq. (14). It is a reasonable first approximation to treat the time window as a single value rather than as a range because the dissociation rate varies exponentially with the excess energy. The narrow instrumental time window kinetically selects those ions that have the requisite energy to dissociate with lifetime τ. No explicit assumption is made about the ion source temperature or the shape of the internal energy distribution of the ions coming from the source, but the ions must be hot enough to include some with energy E_{d}. Combining Eqs. (9) and (14) in terms of $\Delta_{\text{avg}}E$, the internal energy of the ions that have lifetimes equal to the instrumental time window τ can be derived as Eq. (15),

$$E_{\text{d}} = \frac{\Delta_{\text{avg}}E}{1 - (2\nu\tau)^{-1/(s-1)}} \tag{15}$$

where the approximation $E_{\text{d}} - \Delta_{\text{avg}}E \gg \Delta\Delta E/2$ has been used again, for which $k_1(E_{\text{d}})$ and $k_2(E_{\text{d}})$ have the same magnitude.

Combining Eqs. (13) and (15) yields the final approximate expression for the effective temperature, Eq. (16).

$$T_{\text{eff}} \approx \frac{\Delta_{\text{avg}}E}{R(s-1)[(2\nu\tau)^{1/(s-1)} - 1]} \tag{16}$$

To my knowledge, this result has not been reported previously. It states that the effective temperature is directly proportional to the well depth of the cluster and is inversely proportional to the number of degrees of freedom. The product of the reaction frequency and the instrumental time window also directly influences the observed effective temperature via the term in square brackets. The approximations and assumptions in the derivation of Eq. (16) are (1) the classical RRK model, (2) zero reverse activation energies, (3) metastable ion dissociation with a narrow time window, (4) a single cluster lifetime corresponding with a single internal energy (rather than distributions of both), (5) high ion–source temperatures (vide infra), (6) identical frequency factors for the two channels (zero entropy difference), and (7) the restriction that $E_{\text{d}} - \Delta_{\text{avg}}E \gg \Delta\Delta E/2$. The range of validity of this last approximation can be evaluated using Eq. (15) with typical values of $\nu = 10^{13}$ s^{-1}, $\tau = 10^{-5}$ s, $\Delta E_{\text{avg}} = 100$ kJ mol^{-1}, and $\Delta\Delta E = 10$ kJ mol^{-1}. With those parameters, the approximation is reasonable when the number of oscillators is about 20 or higher. For a lower number of degrees of freedom or a shallower well depth, the dissociation rate is rapid and the only cluster ions that survive to reach the

field-free region have internal energies near threshold. In that situation, the effective temperature in Eq. (12) depends on $\Delta\Delta E$, and the kinetic method plot will exhibit significant curvature. This curvature results from the strong energy dependence of the rate constant ratio at energies near threshold.

Eq. (16) gives no dependence of the effective temperature on the ion source temperature, consistent with observations that metastable ion ratios are often independent of the source temperature [1,16]. Source temperature effects are discussed further below.

4. Detailed microcanonical analysis

A rigorous analysis or modeling of real kinetic method experiments should use full Rice-Ramsperger-Kassel-Marcus (RRKM) theory [19,21], as in the work of Brauman and co-workers [11] and Drahos and Vékey [13], but that is not the intention of this work. Instead, I employ classical RRK theory with a detailed kinetic analysis to illustrate the factors that result in the simple functional dependence of the effective temperature given by Eq. (16) and to explore the range of validity of the other assumptions used in its derivation. The qualitative conclusions will also apply to a more quantitative microcanonical unimolecular dissociation rate model.

Bojeson and Breindahl [8] presented the kinetics equations for the ion intensities observed in the kinetic method using metastable ion dissociation. In a metastable ion experiment in a tandem mass spectrometer, the product ion is detected if the metastable cluster dissociates after the time-of-flight t_1 from the ion source through the first mass-selection region to the entrance of the field-free region but before time-of-flight t_2 from the source to the exit of the field-free region. For ion clusters with total internal energy E, the probability of detection of the A_j^- ion, $P_j(E)$, is given by Eq. (17) [8],

$$P_j(E)\ dE = P_0(E)\ \frac{k_j(E)}{k_{\text{tot}}(E)}\left[e^{-k_{\text{tot}}(E)t_1} - e^{-k_{\text{tot}}(E)t_2}\right]\ dE \tag{17}$$

where $k_{\text{tot}}(E) = k_1(E) + k_2(E)$ and $P_0(E)$ is the internal energy distribution of the cluster ions from the ion source. In Eq. (17), the exponential terms in square brackets describe the *kinetic selection* of ions with the correct internal energies to dissociation during the instrument time window. The approximate analysis in the previous section treated the kinetic selection as a delta function at $E = E_d$.

The internal energy distribution of the ions is often ill-defined in mass spectrometry [22], because it depends on the details of the ion source and can also be influenced by energetic collisions in the post-source regions. Bojeson and Breindahl [8] used $P_0(E) = 1$, which assumes that all internal energies are equally probable. That may be a reasonable approximation in the high-temperature limit if the kinetic selection represented by Eq. (17) defines a narrow energy range. Brauman and co-workers [11] used a displaced Boltzmann distribution with zero probability below a fixed energy high above the threshold energies for dissociation. Brauman and co-workers [11] did not consider the exponential kinetics terms in Eq. (17); their fixed energy distribution substitutes to some degree for the kinetic selection, but without properly including the dependence on the rates and instrumental time windows. Drahos and Vékey [13] employed a thermal Boltzmann energy distribution, and I adopt that approach here. Although practical ion sources may yield a non-Boltzmann distribution of internal energies, it is possible in principle to design a source that does produce a true thermal distribution. A Boltzmann distribution of the total internal energies of the ions at source temperature T_s is given by Eq. (18),

$$P_0(E)\ dE = \frac{\rho(E)\ \exp(-E/k_B T_s)\ dE}{Q_0(T_s)} \tag{18}$$

where $\rho(E)$ is the density of states (number of quantum states per unit energy) of the cluster ion at internal energy E and $Q_0(T_s)$ is the partition function of the cluster ion. For the case of the classical RRK model, it is appropriate to use the classical density of states of a collection of s identical harmonic oscillators, Eq. (19) [19,20].

$$\rho(E) = \frac{E^{s-1}}{(s-1)!(h\nu)^s} \tag{19}$$

The classical model is not quantitative, but it gives correct general trends. The total product ion intensity is $P_j(E)$ integrated over all energies, Eq. (20),

$$I_j = I_0 \int_{E=0}^{E=\infty} P_j(E)\ dE \tag{20}$$

where I_0 is the initial intensity of the cluster ions. Combining Eqs. (17), (18), and (20), the complete expression for the ratio of ion intensities is given by Eq. (21),

$$\frac{I_2}{I_1} = \frac{\int_{E=0}^{E=\infty} \rho(E)e^{-E/k_BT_s}\frac{k_2(E)}{k_{tot}(E)}[e^{-k_{tot}(E)t_1} - e^{-k_{tot}(E)t_2}]\,dE}{\int_{E=0}^{E=\infty} \rho(E)e^{-E/k_BT_s}\frac{k_1(E)}{k_{tot}(E)}[e^{-k_{tot}(E)t_1} - e^{-k_{tot}(E)t_2}]\,dE} \tag{21}$$

which applies to any model for the microcanonical rates $k(E)$ and the density of states $\rho(E)$. To reproduce kinetic method plots, the natural logarithm of the intensity ratio from Eq. (21) is calculated as a function of $\Delta\Delta E$. The dependence of the intensity ratio on $\Delta\Delta E$ is implicit in the calculation of the microcanonical rate coefficients, $k_j(E)$. According to Eq. (3), the phenomenological effective temperature is calculated using Eq. (21) from the slope of point $\ln(I_2/I_1)$ at $\Delta\Delta E$ ($\approx\Delta\Delta H$), relative to the origin at $\Delta\Delta E = 0$ where $\ln(I_2/I_1) = 0$. This calculation of the effective temperature parameter is based on what would be observed in an experiment, and does not relate to any thermodynamic temperature.

5. Comparison of the canonical and microcanonical derivations

At this point, it is useful to compare the microcanonical analysis with the canonical treatment given in Eqs. (4)–(7). The canonical rate constant is given by integrating the microcanonical rates over the thermal internal energy distribuiton as shown in Eq. (22),

$$k_j(T^*) = \frac{1}{Q_0(T^*)} \int_{E=0}^{E=\infty} \rho(E)e^{-E/k_BT^*}k_j(E)\ dE \tag{22}$$

where T^* denotes a true thermodynamic temperature. The ratio of thermal rate coefficients for two parallel decomposition channels is given by Eq. (23).

$$\frac{k_2(T^*)}{k_1(T^*)} = \frac{\int_{E=0}^{E=\infty} \rho(E)e^{-E/k_BT^*}k_2(E)\ dE}{\int_{E=0}^{E=\infty} \rho(E)e^{-E/k_BT^*}k_1(E)\ dE} \tag{23}$$

A comparison of Eqs. (21) and (23) shows the distinction between the ratio of thermal rates and the ratio of observed ion intensities. The latter are weighted inside the integrations over the energy distribution by the exponential kinetic terms [in square brackets in Eq. (21)], which effectively selects a slice of the internal energy distribution. The slices do not have sharp energy boundaries, however, because of the random exponential decay lifetimes of clusters of any given internal energy. The kinetic selection of a portion of the initial source internal energy distribution is the key to understanding the dependence of the "effective temperature" on molecular and instrumental parameters, as given approximately by Eq. (16). The selected energies and therefore the effective temperature parameter differ for complexes that have different intrinsic rates, due to the number of degrees of freedom, well depth, or transition state character [13]. Theoretical treatments that use a fixed cluster internal energy or energy distribution [11,12] cannot reproduce these effects.

If the integral in Eq. (22) for the canonical rate is evaluated using the classical RRK expression in Eq. (10) with the classical density of states for a collection of s harmonic oscillators, Eq. (19), the result is the familiar Arrhenius rate expression, Eq. (24) [19,20].

$$k_j(T^*) = \nu \exp(-\Delta_j E_{0K}/k_BT^*) \tag{24}$$

The classical RRK expression is the only form of the microcanonical rate constant for which the Arrhenius

Table 1
Parameters for baseline model calculations

$t_1 = 2 \times 10^{-5}$ s
$t_2 = 4 \times 10^{-5}$ s
$T_s = 500$ K
$\nu = 1 \times 10^{13}$ s ($\nu/c = 334$ cm^{-1})
$s = 30$
$\Delta_{avg}E = (\Delta_2E + \Delta_1E)/2 = 100$ kJ mol^{-1}
$\Delta\Delta E = \Delta_2E - \Delta_1E = 0$

relationship is exact [20]. Arrhenius behavior ensures that the ratio of macroscopic canonical rate coefficients exactly follows Eq. (6), i.e. that the logarithm of the ratio of rates depends linearly on $\Delta\Delta E_{0K}$. Thus, *the classical RRK model is predisposed to meet the assumptions of the kinetic method*. In general, the simple Arrhenius equation does not hold exactly, e.g. for rates calculated using RRKM theory or where quantum tunneling or angular momentum effects are important. Therefore, any deviations from ideal behavior found here using the classical RRK model can only become more pronounced if a more quantitative microcanonical model is employed.

6. Numerical simulations

To test the approximation analytical expression for the effective temperature parameter in Eq. (16) and to examine other aspects of the kinetic method, numerical simulations using the detailed microcanonical analysis given in Sec. 4 are presented here. The effects of various molecular and instrumental parameters on the effective temperature are considered systematically. A set of typical molecular and instrumental parameters for metastable ion dissociation, given in Table 1, is used for baseline model calculations; then various parameters are changed one at a time. The numerical results are summarized in Table 2.

Comparison of T_{eff} calculated by Eq. (16) with the values obtained from numerical simulations (Table 2) shows that the analytical function usually overestimates the effective temperature. This is mainly due to the chosen baseline source temperature of $T_{eff} = 500$ K, which is not in the high-temperature limit for some systems. The worst errors are when T_{eff} from Eq. (16) is greater than T_s, as expected. This occurs for short time windows or long cluster lifetimes (high well depth or large number of oscillators). Excluding those systems where the analytical estimate of T_{eff} is higher than or close to the source temperature, Eq. (16) tracks very well with the numerical simulations, with errors of 0 to + 10%.

Fig. 2 presents data for a system with the baseline model parameters given in Table 1. The top part displays the kinetic method plot of calculated values of $\ln(I_2/I_1)$ versus $\Delta\Delta E$ along with a line representing the ideal linear relationship (tangent of the calculated points near the origin). For this example, the nonlinearity is small—the effective temperature varies from 373 K in the limit of $\Delta\Delta E \rightarrow 0$ to 357 K at $\Delta\Delta E = \pm 10$ kJ mol^{-1}, a 4% deviation. Because $\Delta\Delta E$ is varied while $\Delta_{avg}E$ is held fixed and because $\Delta\Delta S = 0$ in the model, the kinetic method plots are exactly symmetric with respect to inversion about the origin (exchange of the two product channels). The middle part of Fig. 2 shows the RRK rate constants as a function of internal energy for the two channels for a value of $\Delta\Delta E = 8$ kJ mol^{-1}, and the bottom part shows the corresponding internal energy distributions of the ions at the source temperature, $P_0(E)$, and of the dissociating ions, $P_1(E)$ and $P_2(E)$. The latter energy distributions are a narrow slice of the parent distribution and peak at the energy where the rates are comparable to the instrumental time window, as assumed in Eq. (14).

The dependence of the kinetic method plots, rates, and energy distributions on the complexation energy of the cluster and the number of oscillators is shown in Figs. 3 and 4, respectively. As predicted by Eq. (16), the slopes change rapidly with changes in these parameters. As the well depth or the number of degrees of freedom is increased, the dissociation rate becomes slower, and higher internal energy is required for the clusters to dissociate during the fixed instrumental time window. The rates and energy distributions in the middle and bottom parts of Figs. 3 and 4 are calculated for $\Delta\Delta E = 0$, so the two channels have identical rates and internal energy distributions. As shown by the energy distributions

Table 2
Summary of numerical simulations[a]

$\Delta_{avg}E$ (kJ mol^{-1})	s	ν (s^{-1})	t_1 (s)	t_2 (s)	T_s (K)	T_{eff} (K) Eq. (16)	T_{eff} (K) $\Delta\Delta E \rightarrow 0$	T_{eff} (K) $\Delta\Delta E = \pm 10$ kJ mol^{-1}
100	**30**	$\mathbf{1 \times 10^{13}}$	$\mathbf{2 \times 10^{-5}}$	$\mathbf{4 \times 10^{-5}}$	**500**	412	373	357
40						165	165	134
50	20					167	162	127
60						247	241	216
80						329	311	291
120						494	424	412
140						576	460	453
	10					158	144	94
	20					334	304	281
	60					499	448	439
	90					530	472	466
					200	412	200	200
					300	412	292	288
					400	412	347	335
					600	412	387	369
					800	412	401	382
					1000	412	408	388
			1	2		216	205	188
			1×10^{-2}	2×10^{-2}		279	266	246
			1×10^{-4}	2×10^{-4}		370	342	325
			1×10^{-6}	2×10^{-6}		512	433	422
			1×10^{-8}	2×10^{-8}		761	493	491
		1×10^{12}				485	420	407
		1×10^{14}				353	329	311

[a] All input parameters same as boldface values in first row except as indicated.

for the dissociating ions, different internal energies are selected kinetically depending on the cluster lifetime that matches the instrumental time window. For very small cluster ions, e.g. $s = 10$ in Fig. 4, the rates are so fast that the only clusters that survive to reach the field-free region are those that have internal energies very close to the threshold energy of 100 kJ mol^{-1}. When the number of oscillators changes, the amount of internal energy stored in the cluster at a given temperature also changes, as reflected in the energy distributions (Fig. 4). For the smaller clusters, there are relatively fewer ions present in the original ensemble with enough energy to dissociate.

For low values of $\Delta_{avg}E$ or low values of s, the kinetic method plots in Figs. 3 and 4 show significant curvature. Table 2 compares the effective temperatures calculated in the $\Delta\Delta E \rightarrow 0$ limit with those calculated for $\Delta\Delta E = \pm 10$ kJ mol^{-1}. The deviation is an indication of the amount of curvature. The effective temperature decreases with increasing $\Delta\Delta E$, as expected from Eq. (12). The case of $\Delta_{avg}E = 50$ kJ mol^{-1} and $s = 20$ with other parameters as in Table 1 is shown in Fig. 5. Here, T_{eff} varies from 162 K for $\Delta\Delta E \rightarrow 0$ to 127 K at $\Delta\Delta E = 10$ kJ mol^{-1}, a variation of 28%. The parameters used in Fig. 5 are experimentally reasonable for electrostatically bound ion–molecule complexes (without covalent or hydrogen bonding). If s is reduced by a factor of five from the actual number of vibrational modes to obtain reasonable rates from the RRK model [8], $s = 20$ represents a cluster ion of 35 atoms. This analysis implies that great caution should be exercised in applying the kinetic method to small or loosely bound cluster ions.

Figs. 6 and 7 show the dependence of the kinetic method plots, energy distributions, and effective temperature on the ion source temperature. Above a source temperature of about 600 K, there is very little

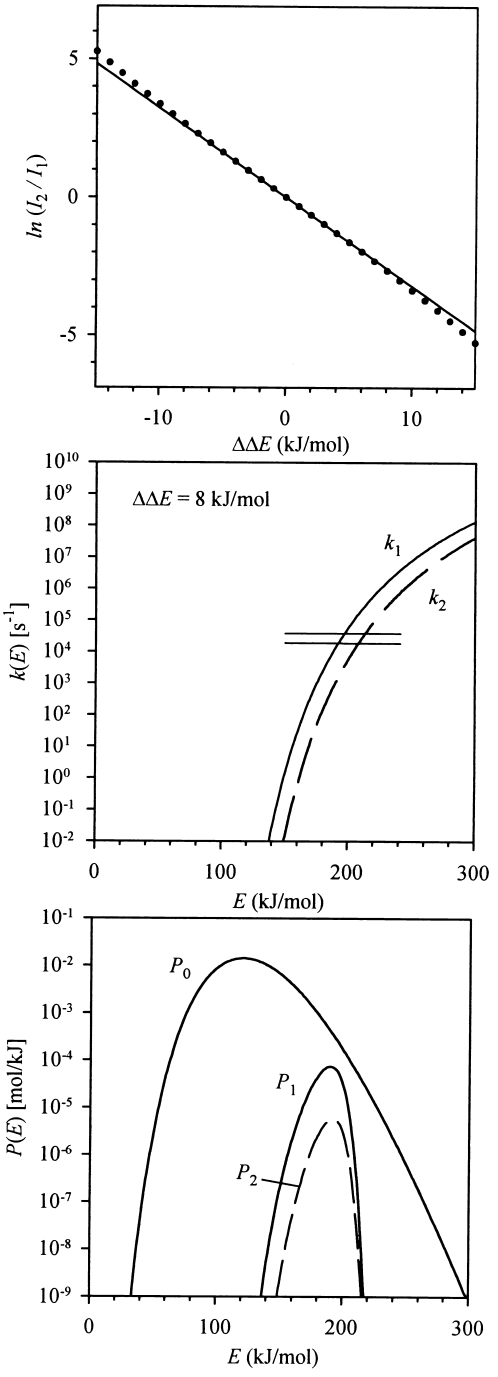

Fig. 2. Numerical simulation of the kinetic method for a system with parameters given in Table 1. Kinetic method plot (top); microcanonical rate coefficients (middle); and energy distributions (bottom) for $\Delta\Delta E$ = 8 kJ mol^{-1}. Horizontal lines mark the instrumental time window (middle).

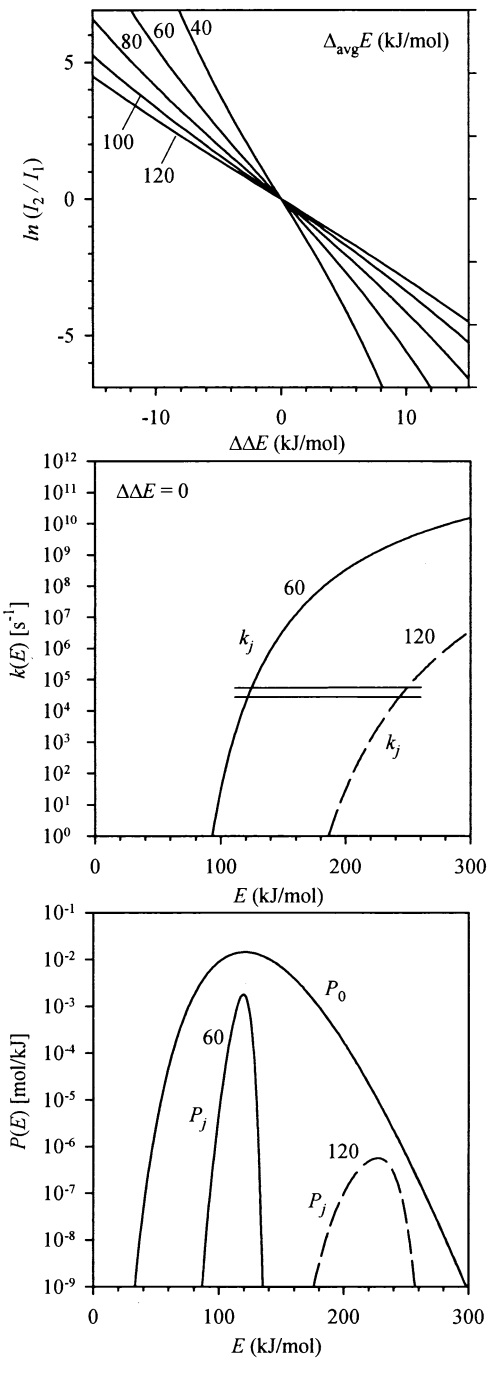

Fig. 3. Numerical simulation of the kinetic method for a system with various values of $\Delta_{avg}E$ (curves labeled in kJ mol^{-1}) and other parameters given in Table 1. Kinetic method plot (top); microcanonical rate coefficients (middle); and energy distributions (bottom) for $\Delta\Delta E$ = 0 kJ mol^{-1}. Horizontal lines mark the instrumental time window (middle).

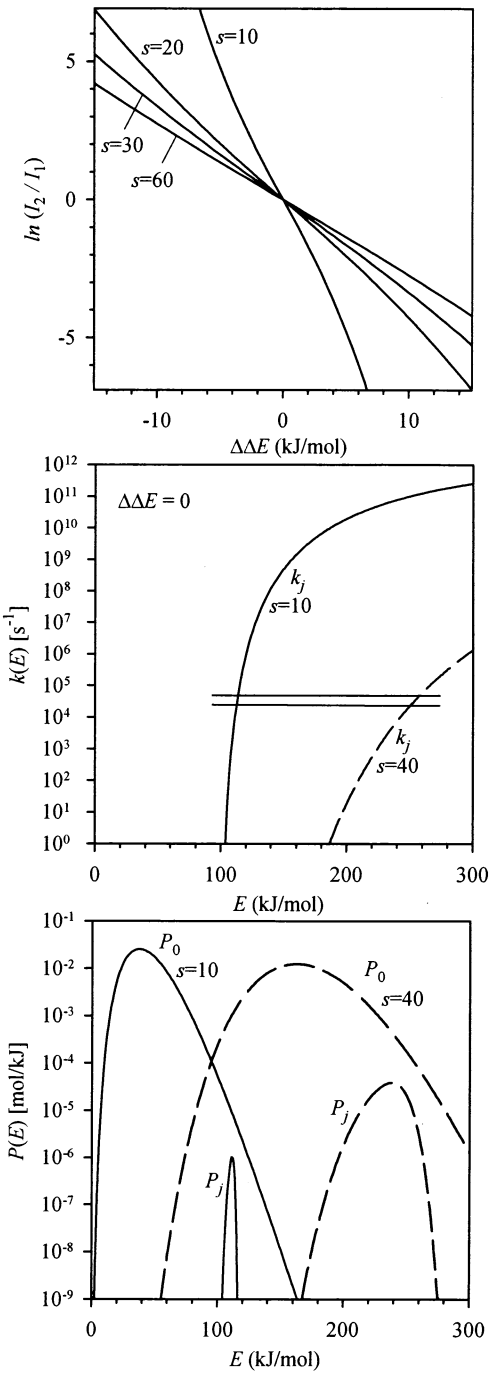

Fig. 4. Numerical simulation of the kinetic method for a system with various values of s (curves labeled) and other parameters given in Table 1. Kinetic method plot (top); microcanonical rate coefficients (middle); and energy distributions (bottom) for $\Delta\Delta E = 0$ kJ mol^{-1}. Horizontal lines mark the instrumental time window (middle).

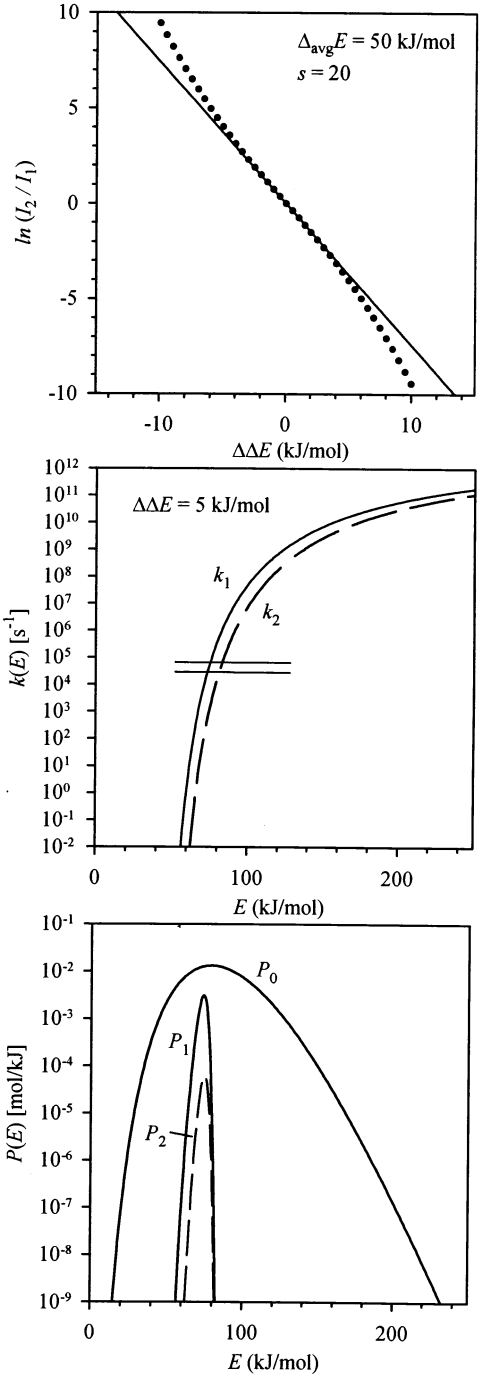

Fig. 5. Numerical simulation of the kinetic method for a system with $\Delta_{avg}E = 50$ kJ mol^{-1}, $s = 20$, and other parameters given in Table 1. Kinetic method plot (top); microcanonical rate coefficients (middle); and energy distributions (bottom) for $\Delta\Delta E = 5$ kJ mol^{-1}. Horizontal lines mark the instrumental time window (middle).

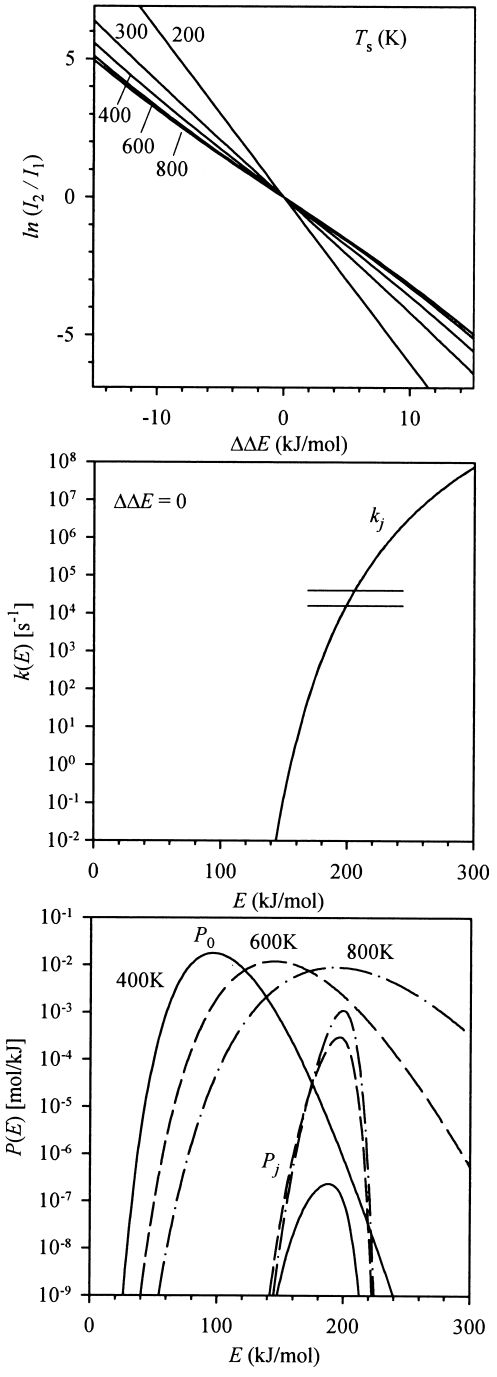

Fig. 6. Numerical simulation of the kinetic method for a system with various values of the source temperature (curves labeled in degrees Kelvin) and other parameters given in Table 1. Kinetic method plot (top); microcanonical rate coefficients (middle); and energy distributions (bottom) for $\Delta\Delta E = 0$ kJ mol^{-1}. Horizontal lines mark the instrumental time window (middle).

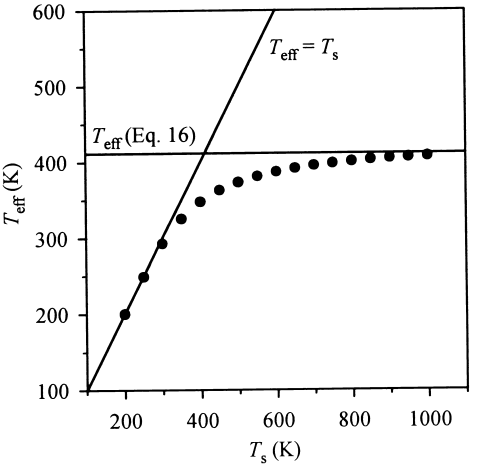

Fig. 7. Dependence of the effective temperature T_{eff} on the ion source temperature T_s for a system with parameters given in Table 1. Numerical simulations (points); analytical expression from Eq. (16) (horizontal line); upper limit of $T_{eff} = T_s$ (slanted line).

change in the effective temperatures and the energy distributions of the dissociating ions. This is consistent with Eq. (16) and with experimental observations that metastable ion intensity ratios are independent of the ion source temperatures [1,16]. The kinetic selection means the same internal energy distribution is responsible for the dissociating ions at any temperature, or with a non-Boltzmann distribution, as long as the parent distribution of energies is high enough to include that energy range and broad enough not to skew the distribution. At low source temperatures, however, the energy distribution of dissociating ions is cut off by the exponential fall-off of the Boltzmann distribution (Fig. 6). Therefore, the source temperature is an upper limit for the effective temperature, as also discussed by Drahos and Vékey [13]. This is shown clearly in Fig. 7, a plot of the effective temperatures versus the source temperature. Fig. 7 also compares the numerical calculations with the analytical expression for the effective temperature. It shows that Eq. (16) is quantitatively valid only for high source temperatures. If Eq. (16) gives a higher temperature than the true source temperature for a thermal source, the latter should be taken as the effective temperature. Conversely, if the observed effective temperature in a metastable ion dissociation

experiment is substantially higher than the apparent source temperature, it indicates that the ions actually have higher internal energies. That could be caused, for example, by activation from collisions between the ion source and the first mass analysis region.

Eq. (16) also indicates that the effective temperature depends on the instrumental time window, as illustrated in Fig. 8 where t_1 is varied and $t_2 = 2t_1$. The time windows of 10^{-8} s to 1 s span the range of time-of-flight, double sector, triple quadrupole, and ion cyclotron resonance mass spectrometers. The slopes of the kinetic method plots show a strong dependence on the time window, and the energy distributions for the dissociating ions shift according to where $k(E)$ intersects the various time windows. Because the time window is generally fixed in a particular experiment, this is not a major concern for application of the kinetic method. For the longer time windows, higher curvature in the kinetic method plots is observed because only ions with energies near threshold survive until time t_1. Variation of the reaction frequency factor, ν, has an inverse effect as changing the instrumental time window.

7. Discussion

The analytical expression for the effective temperature derived here as Eq. (16) shows that the effective temperature parameter depends directly on the well depth of the cluster ion and inversely on the size of the ion. A strong dependence on the product of the reaction frequency and the instrumental time window is also found. A general dependence of the effective temperature on some of these parameters has been noted in previous theoretical and experimental work [8,9,11,13,15,17,23,24]. The approximate expression derived here shows their interrelationships in a useful simple form for the case of metastable ion dissociation. If one used the more sophisticated RRKM theory instead of the classical RRK model, the reaction frequency and the number of oscillators would not be separable quantities. However, the same effects would be contained in the direct calculation of the quantum sums and densities of states, giving an analogous strong dependence of the effective temperature on the number of low-frequency vibrational modes in the cluster ion. The detailed simulations presented here show that the simple analytical relationship derived for the effective temperature, Eq. (16), is a reasonable approximation for small values of $\Delta\Delta E$ and at high source temperatures. For ion clusters that are loosely bound (small average well depth) or have few low-frequency vibrational modes (small effective number of oscillators), there is substantial curvature in the kinetic method plots.

The model used here specifically excludes entropy effects, $\Delta\Delta S = 0$. Therefore, the nonideal behavior observed in the numerical simulations are in addition to deviations that might be caused by entropy effects. Furthermore, because the classical RRK model exactly satisfies the Arrhenius rate relationship, the numerical simulations represent a "best-case scenario" for applicability of the thermodynamic formulation of the kinetic method, Eq. (7).

How important are the nonideal effects for actual experiments? The explicit way to investigate that for a particular system would be to perform quantitative statistical calculations, as has recently been advocated [14] and demonstrated [13] but argued as unnecessary [15]. However, some generalizations can be made based on the present results. Specifically, Eq. (16) can be used in a sensitivity analysis of the effect of various parameters on the effective temperature and on the measured thermochemical quantities.

The effective temperature is directly proportional to the average well depth. For ion clusters of similar compounds, the average complexation energies are often similar, but show some variation. For example, 62 proton-bound amine cations of the type $B_1HB_2^+$ have mean complexation enthalpies [25] of $\Delta_{avg}H = 87$ kJ mol^{-1} with a $\pm 2\sigma$ distribution of ± 11 kJ mol^{-1}, or equivalently $\pm 13\%$ in the effective temperature. Other classes of compounds may exhibit more or less variation in complexation energies. The effective temperature is inversely dependent on $s - 1$ in the RRK model. Frequently, kinetic method comparisons are made for species that vary by substitution of a functional group. Consider as a conservative example a proton-bound phenoxide dimer, $[(RO)(PhO)H]^-$,

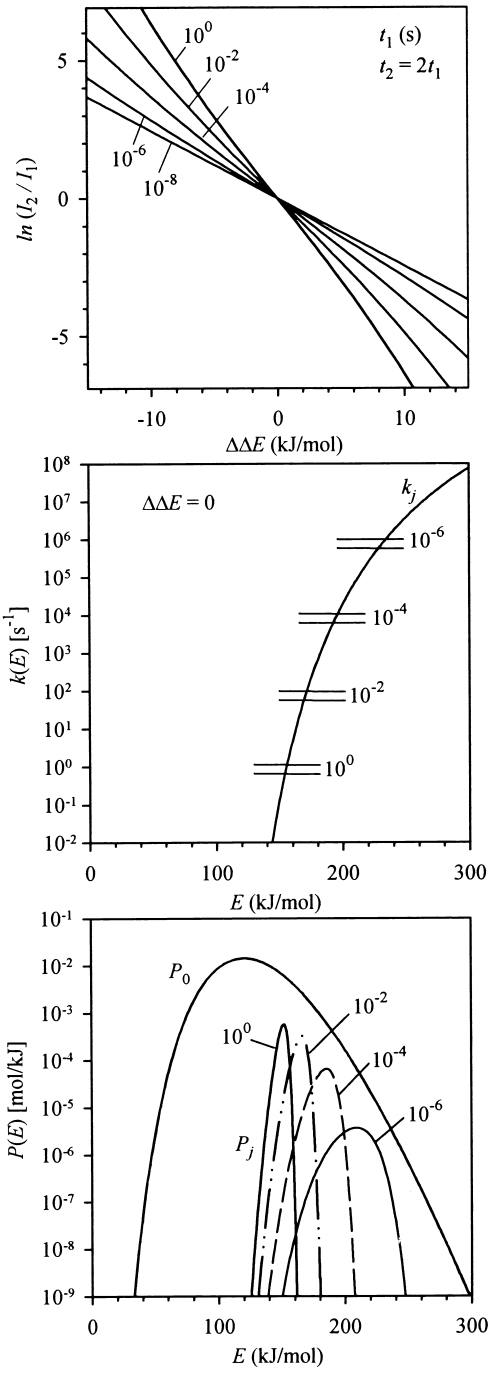

Fig. 8. Numerical simulation of the kinetic method for a system with various time windows defined by t_1 (curves labeled in seconds), $t_2 = 2t_1$, and other parameters given in Table 1. Kinetic method plot (top); microcanonical rate coefficients (middle); and energy distributions (bottom) for $\Delta\Delta E = 0$ kJ mol^{-1}. Horizontal lines mark the instrumental time windows (middle).

where ROH is *p*-methoxyphenol or *m*-fluorophenol, whose gas phase acidities differ from phenol by +5 and −5 kJ mol^{-1}, respectively [26]. The methoxy-substituted cluster has an additional 4 atoms and 12 vibrational modes compared with the fluoro-substituted cluster, giving a ratio of ($s - 1$) of 68:80, or a change of 18% in the effective temperature. The calculated curvature effects can cause T_{eff} to vary for different values of $\Delta\Delta E$. The worst cases are for small clusters, up to a 53% change in T_{eff} from $\Delta\Delta E = 0$ to 10 kJ mol^{-1} (Table 2), but variations up to 10% are common for medium-to-large systems.

In summary, the well depth, size, and curvature effects can *each* be expected to cause variations of 10–20% in the effective temperature from one dimer pair to the next even in fairly well-behaved systems. Such errors might not be independent of each other because of possible correlations between size and well depth. Thus, a relative uncertainty of 20–40% in the effective temperature and therefore in individual relative $\Delta\Delta H$ or $\Delta\Delta G$ measurements appears to be indicated. For a 10 kJ mol^{-1} energy difference between the two channels, that implies an uncertainty of 2–4 kJ mol^{-1}, which is encouragingly small in an absolute sense. Because *relative* enthalpies and Gibbs energies obtained by the kinetic method have frequently been reported to a precision of 0.4 kJ mol^{-1} (0.1 kcal mol^{-1}) [2,27–33], however, intrinsic errors of 2–4 kJ mol^{-1} in individual measurements are significant. Because cluster size and well depth could be correlated with the thermochemical quantity being measured, using multiple references might not always reduce the errors. The *absolute* accuracy of the kinetic method, reported as ±8 kJ mol^{-1} for gas phase acidities, basicities, and proton affinities for example [3], is mainly dependent on the absolute anchoring of the reference species and is not under consideration here. Uncertainties of that magnitude in the anchoring points may mask deviations of relative measurements in calibration experiments.

8. Conclusions

This work presents an approximate analytical expression, Eq. (16), for the effective temperature in the kinetic

method. It is based on the classical RRK model for the microcanonical rate constant and is valid for metastable ion dissociation for small values of the energy difference between the two dissociation channels and for high source temperatures. The model is a best-case scenario because it assumes there are no entropy effects and because the classical RRK model follows the Arrhenius relationship exactly. The main parameters that affect the effective temperature are the cluster complexation energy, the size of the cluster ion, the reaction frequency or preexponential factor, and the experimental time window. Although a near-linear relationship is found between the logarithm of the observed product ion intensity ratio and the energy difference of the two channels, as assumed by the kinetic method, there are significant nonideal curvature effects especially for small or weakly bound clusters. The ion source temperature has a small effect if it is substantially higher than the calculated effective temperature, and the cluster ion internal energy distribution need not be Boltzmann as long as it is broad. The analytical expression for the effective temperature, although not quantitative, provides a means to estimate possible errors based on variation of these parameters.

Acknowledgement

This work was supported by the U.S. Department of Energy, Office of Basic Energy Sciences, grant DE-FG03-97ER14750.

References

[1] S.A. McLuckey, D. Cameron, R.G. Cooks, J. Am. Chem. Soc. 103 (1981) 1313.
[2] R.G. Cooks, J.S. Patrick, T. Kotiaho, S.A. McLuckey, Mass Spectrom. Rev. 13 (1994) 287.
[3] R.G. Cooks, P.S.H. Wong, Acc. Chem. Res. 31 (1998) 379.
[4] R.A. Seburg, R.R. Squires, Int. J. Mass Spectrom. Ion Processes 167/168 (1997) 541.
[5] P.G. Wenthold, J. Hu, R.R. Squires, J. Am. Chem. Soc. 118 (1996) 11865.
[6] S.A. McLuckey, Org. Mass Spectrom. 19 (1984) 545.
[7] F. Greco, A. Liguori, G. Sindona, N. Uccella, J. Am. Chem. Soc. 112 (1990) 9092.
[8] G. Bojesen, T. Breindahl, J. Chem. Soc., Perkin Trans. 2 1994 (1994) 1029.
[9] S. Campbell, E.M. Marzluff, M.T. Rodgers, J.L. Beauchamp, M.E. Rempe, K.F. Schwinck, D.L. Lichtenberger, J. Am. Chem. Soc. 116 (1994) 5257.
[10] H.-F. Grützmacher, A. Caltapanides, J. Am. Soc. Mass Spectrom. 5 (1994) 826.
[11] S.L. Craig, M. Zhong, B. Choo, J.I. Brauman, J. Phys. Chem. A 101 (1997) 19.
[12] T. Zhang, D.P. Ridge, Proceedings of the 46th ASMS Conference on Mass Spectrometry and Allied Topics, American Society for Mass Spectrometry, Orlando, FL, 1998, p. 788.
[13] L. Drahos, K. Vékey, J. Mass Spectrom. 34 (1999) 79.
[14] P.B. Armentrout, J. Mass Spectrom. 34 (1999) 74.
[15] R.G. Cooks, J.T. Koskinen, P.D. Thomas, J. Mass Spectrom. 34 (1999) 85.
[16] J.L. Holmes, C. Aubry, P.M. Mayer, J. Phys. Chem. A 103 (1999) 705; 103 (1999) 6492.
[17] K. Norrman, T.B. McMahon, Int. J. Mass Spectrom. 176 (1998) 87.
[18] K. Norrman, T.B. McMahon, Int. J. Mass Spectrom. 182/183 (1999) 381.
[19] T. Baer, W.L. Hase, Unimolecular Reaction Dynamics: Theory and Experiments, Oxford University Press, New York, 1996.
[20] J.I. Steinfeld, J.S. Francisco, W.L. Hase, Chemical Kinetics and Reaction Dynamics, 2nd edn. Prentice-Hall, Upper Saddle River, NJ, 1998.
[21] R.G. Gilbert, S.C. Smith, Theory of Unimolecular and Recombination Reactions, Blackwell Scientific, Boston, 1990.
[22] K. Vékey, J. Mass Spectrom. 31 (1994) 445.
[23] B. Bogdanov, M. Peschke, D.S. Tonner, J.E. Szulejko, T.B. McMahon, Int. J. Mass Spectrom. 185/186/187 (1999) 707.
[24] G. Chen, R.G. Cooks, D.M. Bunk, M.J. Welch, J.R. Christie, Int. J. Mass Spectrom. 185/186/187 (1999) 75.
[25] D.H. Aue, M.T. Bowers, in Gas Phase Ion Chemistry, M.T. Bowers (Ed.), Academic, New York, 1979, p. 1.
[26] J.E. Bartmess, Negative Ion Energetics Data, in NIST Chemistry WebBook, NIST Standard Reference Database Number 69, W.G. Mallard, P.J. Linstrom (Eds.), National Institute of Standards and Technology, Gaithersburg, MD, Nov. 1998 (http://webbook.nist.gov).
[27] T.K. Majumdat, F. Clairet, J.-C. Tabet, R.G. Cooks, J. Am. Chem. Soc. 114 (1992) 2897.
[28] S. Ma, P. Wong, S.S. Yang, R.G. Cooks, J. Am. Chem. Soc. 118 (1996) 6010.
[29] J. Schwarz, R. Wesendrup, D. Schröder, H. Schwarz, Chem. Ber. 129 (1996) 1463.
[30] M.N. Eberline, T. Katiaho, B.J. Shay, S.S. Yang, R.G. Cooks, J. Am. Chem. Soc. 1994 (1994) 2457.
[31] S.H. Hoke II, S.S. Yang, R.G. Cooks, J. Am. Chem. Soc. 116 (1994) 4888.
[32] Z. Wu, C. Fenselau, J. Am. Soc. Mass Spectrom. 3 (1992) 863.
[33] G. Boand, R. Houriet, T. Gäumann, J. Am. Chem. Soc. 105 (1983) 2203.